

Spatiotemporal Intracellular Nitric Oxide Signaling Captured Using Internalized, Near-Infrared Fluorescent Carbon Nanotube Nanosensors

Zachary W. Ulissi,^{†,#} Fatih Sen,^{†,‡,§} Xun Gong,^{‡,§} Selda Sen,[†] Nicole Iverson,[†] Ardemis A. Boghossian,^{†,¶} Luiz C. Godoy,[§] Gerald N. Wogan,[§] Debabrata Mukhopadhyay,^{‡,||} and Michael S. Strano*,[†]

[†]Department of Chemical Engineering, Massachusetts Institute of Technology, Cambridge, Massachusetts 02139, United States

[‡]Department of Biomedical Engineering and Physiology, Mayo College of Medicine, Rochester, Minnesota 55905, United States

[§]Department of Biological Engineering, Massachusetts Institute of Technology, Cambridge, Massachusetts 02139, United States

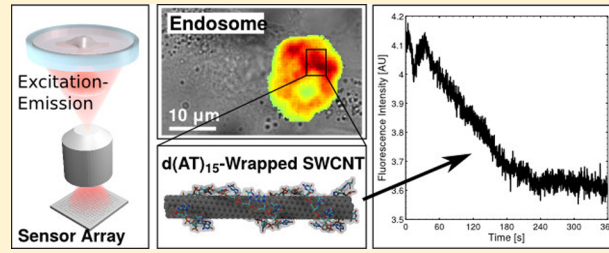
[¶]Department of Biochemistry and Molecular Biology, Mayo College of Medicine, Rochester, Minnesota 55905, United States

^{||}Department of Biochemistry, Dumlupınar University, Kutahya, 43100, Turkey

Supporting Information

ABSTRACT: Fluorescent nanosensor probes have suffered from limited molecular recognition and a dearth of strategies for spatial-temporal operation in cell culture. In this work, we spatially imaged the dynamics of nitric oxide (NO) signaling, important in numerous pathologies and physiological functions, using intracellular near-infrared fluorescent single-walled carbon nanotubes. The observed spatial-temporal NO signaling gradients clarify and refine the existing paradigm of NO signaling based on averaged local concentrations. This work enables the study of transient intracellular phenomena associated with signaling and therapeutics.

KEYWORDS: Single-walled carbon nanotube, nitric oxide, sensor, photoluminescence



Nitric oxide (NO) is integral to the vascular system as a vasodilator, the nervous system as a neurotransmitter and the immune system as a defensive agent,^{1,2} but it also plays an integral role in pathology, specifically for inflammatory diseases, vascular diseases, diabetes, and cancer.^{3–6} Currently, NO detection in tissues is limited to assays developed to detect downstream products of NO. However, these assays fail to elucidate the implications of fluctuating intracellular NO levels.

Many techniques have been developed to quantify nitric oxide levels in biological settings. Two common approaches are the use of small-molecule labeling dyes^{7–13} and specially coated electrodes.^{14–18} Dyes are usually delivered intracellularly or in the interstitia where they bind reactive species and indicate species concentration through either fluorescence or chemiluminescence. However, dyes such as the widely used 4,5-diaminofluorescein respond to all species that nitrosate the substrate, including many NO decomposition products. Such dyes can also react with dehydroascorbic acid and ascorbic acid to yield emission products with similar emission wavelengths, interfering with NO detection.¹⁹ These dyes are also non-reversible, suffer from chemical photobleaching inherent to small-molecule fluorophores, and generally cannot be resolved at a sufficient level to measure NO at subcellular spatial resolution. Electrochemical measurement, however, is capable of detecting absolute NO levels but it cannot map the

subcellular space. Hence, none of these methods to date have enabled the detection of intracellular NO dynamics.

Molecular sensors based on nanoscale structures are well suited to address many of these limitations with examples including sensors based on quantum dot FRET probes,²⁰ graphene oxide probes,²¹ aggregating gold nanorods and nanoparticles,²² and single-walled carbon nanotubes (SWCNTs). SWCNTs have been shown to be particularly well-suited as intracellular nitric oxide sensors. SWCNTs have a very strong photoluminescence (PL) response, absorbing and emitting in the visible and near-infrared (nIR) spectra, respectively. Small-molecule analytes can interrupt the PL emission by providing a site for generated excitons to recombine destructively. This results in an easily observable quenching and in the case of NO, single-molecule detection as individual molecules adsorb to the surface.²³ Various polymers or DNA corona phases can wrap the outer surface of the SWCNT to enable selective molecular detection of other analytes by restricting molecular access to the SWCNT surface. With this method, we have designed sensors specific for glucose,^{24–27} DNA,^{28–31} ATP,²³ H₂O₂,^{32,33} and NO.^{23,34} Such sensors have also been demonstrated for whole-animal

Received: June 21, 2014

Published: July 16, 2014

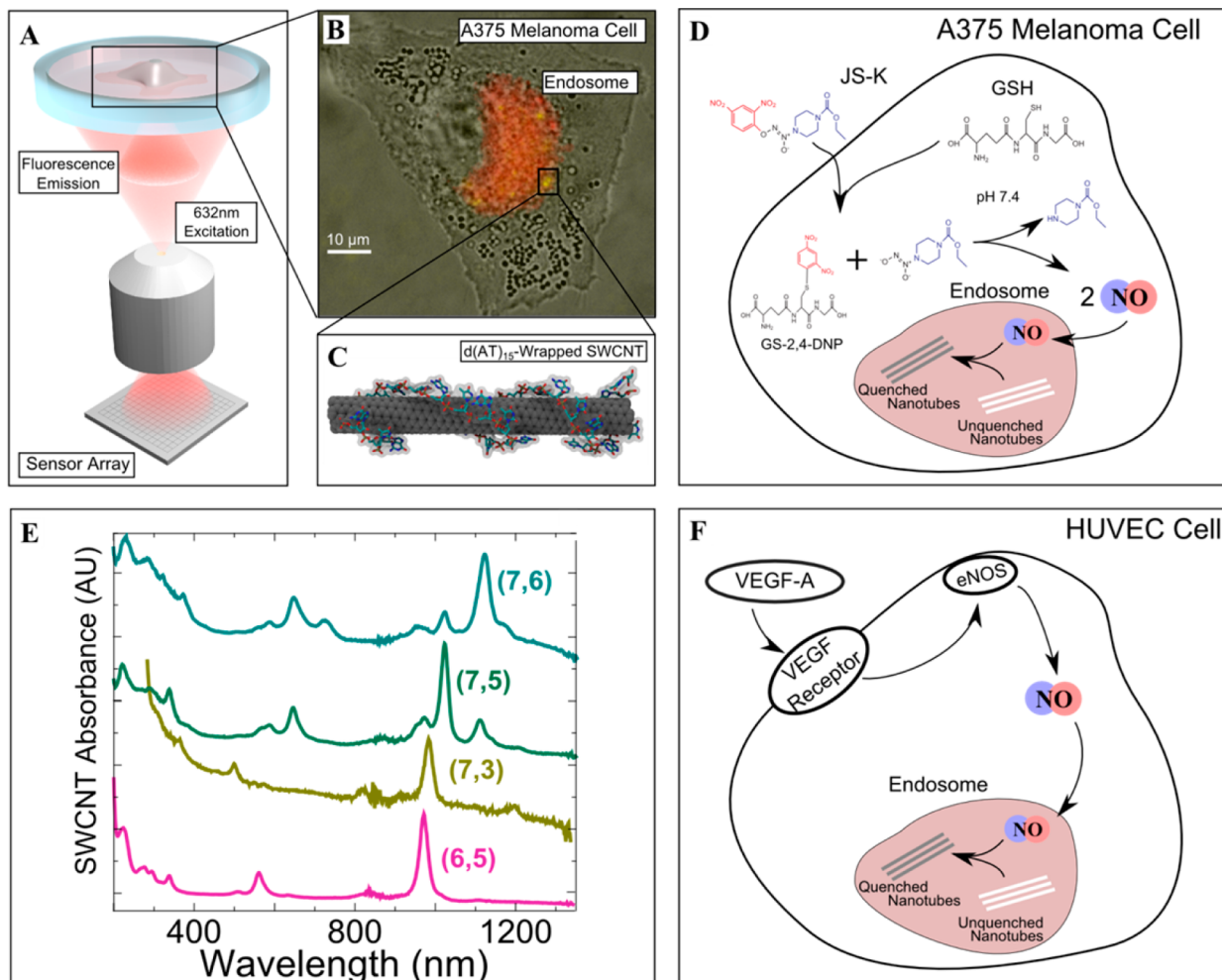


Figure 1. Experimental setup for the detection of intracellular NO. (A) The fluorescence setup with an A375 melanoma cell of interest located on a Petri dish, a 632 nm excitation source, and a nIR sensor array. (B) Co-localization of the SWCNT sensors (yellow) with the cell endosomes (red) as indicated using Lysotracker Red. (C) A cartoon of a DNA(AT)₁₅-wrapped SWCNT capable of detecting NO. (D) Chemical pathway for the penetration and decomposition of JS-K, resulting in increased NO concentrations in the endosome. (E) Absorbance spectra for four SWCNT chiralities. (F) Chemical pathway for the binding of VEGF-A to VEGF receptors on HUVEC cells, causing a release of NO from eNOS bound to the cell membrane.

measurements³⁵ but have not been studied for their ability to do spatiotemporal sensing at the subcell length scale.

In this work, we utilize the SWCNT-based NO sensor and a new methodology to study NO generation and intracellular signaling for the first time. Such sensors are readily internalized by A375 melanoma cells through macropinocytosis,³⁶ exhibit low background signals and have a high signal-to-noise ratio that allows for real time detection of intracellular spatiotemporal NO. NO generation and subsequent intracellular signaling was assayed using the NO releasing anticancer drug JS-K in the A375 melanoma cells. Endogenous NO generation from vascular endothelial growth factor (VEGF) stimulation of human umbilical vein endothelial cells (HUVECs) was also measured. We show that the resulting spatial and temporal fluctuations can only arise from two or more asynchronous NO sinks within the cell that are spatially distinct. This finding provides a more in-depth understanding of intracellular NO and illustrates just one use of these nanosensor probes and their capability to expand the knowledge of biological molecules and their intracellular distribution.

While it is currently believed that the local average concentration of NO governs its pathophysiology, some studies

have indicated the importance of intracellular NO localization.³⁷ With the novel SWCNT sensor for NO, we demonstrate that NO concentration is dynamically modulated at an intracellular level, leading to a more complex picture of NO signaling and biochemistry. It is shown that spatiotemporal fluctuations can only be a consequence of temporally varying NO sinks within the cell, and that two or more asynchronous sinks must be present to model the observations. These results offer new possibilities to explore and understand NO signaling. For our future work, the unique PL emissions of different SWCNT chiralities can be utilized for the simultaneous study of multiple substrates and their dynamic interactions.

SWCNT Uptake and Colocalization in Melanoma Cells. d(AT)₁₅-DNA wrapped SWCNTs previously found to selectively detect nitric oxide in vitro²³ were prepared and introduced to cultures of A375 melanoma cells (see Supporting Information Methods). The SWCNT concentration was quantified via absorbance spectroscopy, and a concentration of 2 μg/mL was diluted into media for cellular uptake. After introduction of the SWCNTs and a 12 h incubation, the cells were found to have internalized the SWCNTs. SWCNT PL was observed using a previously described nIR fluorescence

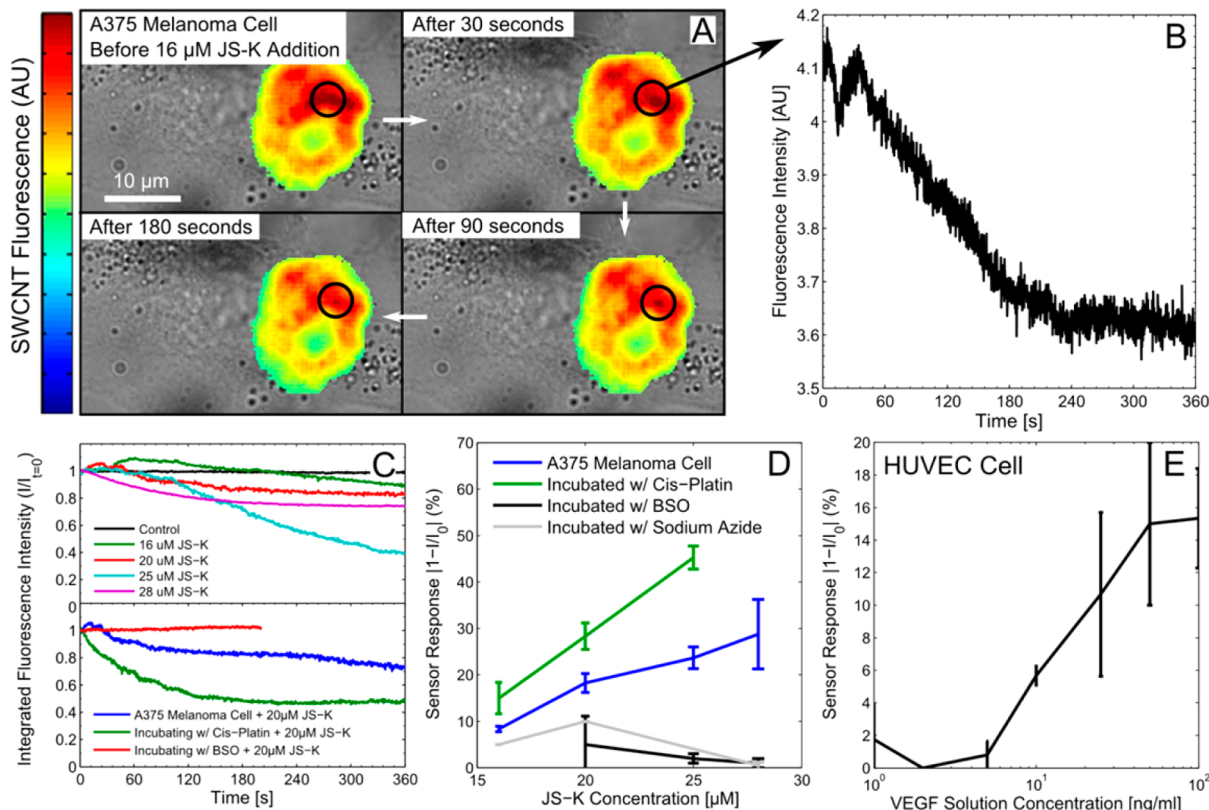


Figure 2. Confirmation of Intracellular NO Detection. (A) nIR intensity profiles of the endosome region over 3 min after exposure to JS-K, showing gradual intensity quenching. (B) Intensity of a single point over time showing rapid quenching followed by a settling to a new steady state intensity. (C) Quenching profiles for several JS-K concentrations, and confirmation of the included literature JS-K pathway by promoting the intermediate reagent GSH with Cisplatin or reducing GSH with buthionine sulfoximine (BSO). (D) Calibration curves showing the final quenching response to various JS-K concentrations after incubation with Cisplatin, BSO, or sodium azide. (E) A similar calibration curve for a HUVEC cell exposed to vascular endothelial growth factor (VEGF).

microscope setup²³ (Figure 1A). Briefly, SWCNTs were excited with a 632 nm laser (CrystaLaser, CL660-100, 100 mW), and fluorescent emission was monitored in an inverted microscope (Carl Zeiss, Axiovert 200) using a 100x TIRF objective and a two-dimensional (2D) liquid nitrogen-cooled InGaAs near-infrared sensor array (Princeton Instruments OMA 2D). nIR images were saved every 0.2 s over the course of an experiment. The absorbance spectra for four SWCNT chiralities³⁸ is shown in Figure 1E.

The intracellular presence and location of the SWCNTs was confirmed through optical and fluorescent microscopy. The SWCNT nIR emission was observed in the perinuclear region, indicative of a late endosome and lysosome localization. This was further confirmed through incubation with Lysotracker Red, which colocalized with the nIR image (Figure 1B). SWCNT sensors were shown to respond through the direct administration of nitric oxide to the cell medium (see Supporting Information), but this method was not used extensively because of the short diffusion length, roughly 20 μm,³⁹ and cellular barriers from large nitric oxide concentration gradients in and near cells. MAHMA NONOate [(Z-1-N-methyl-N-[6-(N-methylammoniohexyl)amino]diazen-1-iium-1,2-diolate)] was also attempted for NO introduction (see Supporting Information) but release occurred outside of the cell, diluting its effect. Instead, we relied on the production of intracellular nitric oxide using the nitric oxide pro-drug JS-K.

Nitric Oxide Signaling Dynamics in Response to the Glutathione Activated Donor JS-K. The nitric oxide pro-

drug JS-K⁴⁰ [O2-(2,4-dinitrophenyl)-1-[(4-ethoxycarbonyl)-piperazin-1-yl]diazen-1-iium-1,2-diolate] was utilized to exogenously generate intracellular NO concentrations and signaling. JS-K reacts with intracellular glutathione (GSH) to produce an intermediate (4-carbethoxy-PIPERAZI/NO) that then releases two parts NO for each JS-K molecule (Figure 1D). This additional nitric oxide can then freely diffuse throughout the cell and its intracellular location detected with our SWCNT sensors. This mechanism was verified first by modulating the JS-K concentration and then modulating the intracellular GSH concentrations to alter net nitric oxide production.

The degree of SWCNT quenching in A375 melanoma cells was found to increase with increasing JS-K concentrations in the range of 16–28 μM (Figure 2). For a given JS-K concentration, the baseline integrated SWCNT PL intensity of a target cell was observed for 400 s. JS-K was then added to the cell medium, and the PL levels of the same cell were imaged over another 400 s, which was typically sufficient for the quenching to reach steady state (Figure 2A). The PL at local maxima (central SWCNT positions) were also found to decrease in a similar manner (Figure 2B). Data for each JS-K concentration represent the results of three replicates unless otherwise stated. Examples of the PL changes over 3 min for each tested JS-K concentration (16, 20, 25, and 28 μM) are shown in Figure 2C, and the final quenched intensity for each concentration is shown in Figure 2D. To ensure the introduced dimethyl sulfoxide (DMSO) solution was not responsible for the PL changes, a stock DMSO solution was added instead and

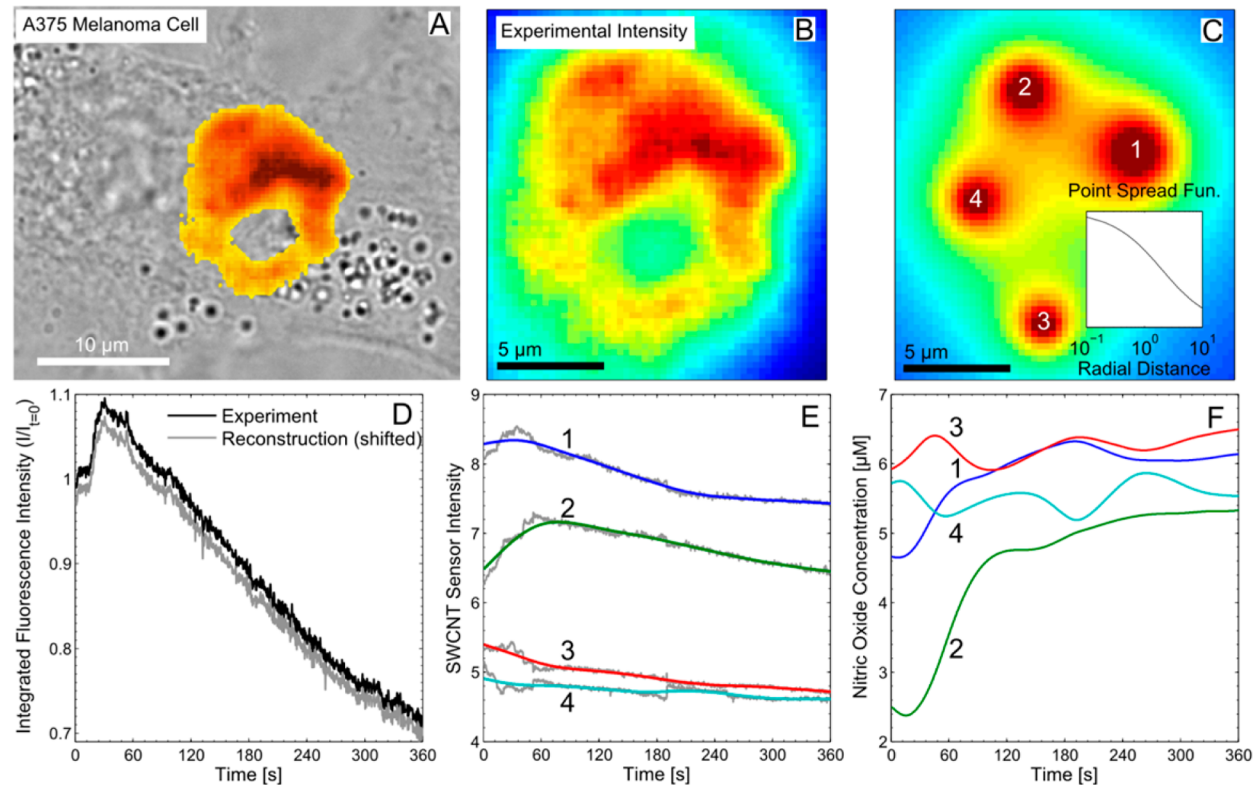


Figure 3. Calculation of intracellular nitric oxide concentration through observations of SWCNT fluorescence. (A) Fluorescence intensity of SWCNT in A375 melanoma cell. (B) Experimental intensity profile. (C) Reconstructed intensity profile after fitting a small number of point illumination sources with point spread functions indicated in the inset. (D) Demonstration that point-source process retains the same total intensity information from Figure 2. (E) Intensity for each point source, before and after removal of high frequency noise with a smoothing spline. (F) Calculated nitric oxide concentration for each point source using a kinetic model for the adsorption/desorption of nitric oxide on SWCNT.

no PL change observed (see Supporting Information Note 3). The protocol for JS-K administration and NO release was qualitatively confirmed through the administration of the commercial NO-sensitive fluorescent dye DAF-FM (see Supporting Information Note 6). It is important to note that in contrast to diaminofluoreceins, SWCNT NO sensors react with NO directly and do not involve reactive oxygen species nor NO byproducts.

We investigated NO dynamics in the presence of both elevated and suppressed GSH. Intracellular GSH levels were measured using a GSH assay (see Supporting Information Methods) with a measured concentration of 1.3 ± 0.3 mM inside the A375 melanoma cells. Incubating the cells with Cisplatin (see Supporting Information Methods), a chemotherapeutic agent that cross-links DNA increasing cellular stress and GSH production,⁴¹ resulted in an increased GSH concentration of 3.2 ± 0.4 mM and increased PL quenching for each concentration of JS-K tested (Figure 2D). Conversely, incubating the cells with buthionine sulphoximine (BSO), an inhibitor of gamma-glutamylcysteine synthetase that reduces GSH concentrations,⁴² resulted in a decreased GSH concentration of 0.71 ± 0.24 mM and less PL quenching (Figure 2D). Finally, administering sodium azide disabled aerobic metabolism in the melanoma cells and effectively removed their ability to produce GSH. Subsequent addition of JS-K resulted in no observable quenching of the SWCNT PL (Figure 2D).

Application to Vascular Endothelial Growth Factor and HUVEC Cells. To examine our hypothesis in a different system, vascular endothelial growth factor (VEGF)-mediated NO production was monitored in endothelial cells. HUVEC

cells were observed to uptake the SWCNT sensors using the same incubation protocol as the A375 melanoma cells. Introducing VEGF activates endothelial nitric oxide synthase (eNOS)⁴³ resulting in an increase in intracellular NO concentration and a detectable quenching of the SWCNT PL, as illustrated in Figure 1F. PL quenching was tested for VEGF treatments ranging from 1 ng/mL to 100 ng/mL. Responses were observed at the widely accepted treatment concentration of 10 ng/mL (Figure 2E). Furthermore, VEGF stimulated NO release occurs more rapidly with larger intracellular gradients, illustrating the differences between physiological and pharmacological NO release (see Supporting Information).

Spatiotemporal Mapping of Intracellular Nitric Oxide.

To interpret the resulting novel data sets, we developed an absorption/scattering image processing algorithm for allowing spatial and temporal data to be extracted from movies of cellular quenching during NO signaling, which we demonstrate for the case of an A375 melanoma cell responding to JS-K. The d(AT)₁₅-DNA wrapped SWCNT sensors allow for spatiotemporal resolution of nitric oxide concentrations not possible with previous NO detection mechanisms. Inside the cell, the SWCNTs are localized to multiple endosomes resulting in multiple effective sensors within the cell. Each SWCNT bundle within an endosome functions as a point source of photoluminescent light in the NIR scattering and absorbing cell, effectively illuminating the surrounding region (Figure 3A,B). The SWCNT centers and intensities were reconstructed using a simple NIR scattering/absorption model, and the resulting intensity traces were analyzed to calculate the observed nitric

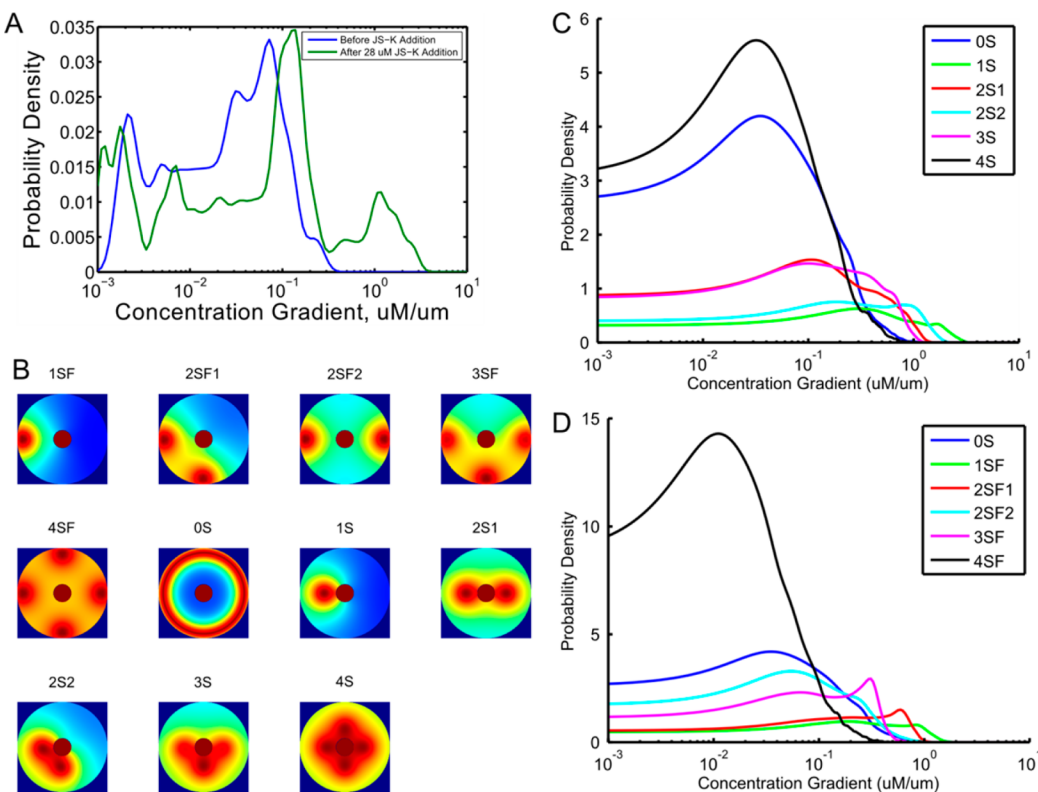


Figure 4. Observed intracellular NO gradients and a numerical model for the release of NO by JS-K addition. (A) Typical observed NO concentration gradients between sensor regions before and after the introduction of 28 μM JS-K. Baseline concentration differences are approximately 0.1 $\mu\text{M}/\text{um}$. A second peak in the histogram at approximately 1 $\mu\text{M}/\text{um}$ occurs at the beginning of the experiment, before the SWCNT settle to a new equilibrium. (B) Diffusion-reaction model simulation of intracellular NO formation with 16 μM JS-K addition. Zero to four sources of intracellular GSH are placed in various locations. The system is optimized such that NO concentration is approximately 4 μM , and the gradient is studied. (C,D) For each scenario in B, the gradient is calculated as the concentration difference collected at random pairs of locations within 3 μm of the nucleus normalized by distance. A probability density distribution is then plotted. Results show that at least one source is required to reproduce the concentrations and gradients.

oxide signal using known kinetics for SWCNT PL quenching by NO.

Each SWCNT bundle is treated as a point illumination source. The propagation of nIR light in tissue and cells is effectively modeled at steady state by solving the Helmholtz equation for a scattering/absorbing medium

$$\mu_a \phi(r) - \frac{1}{3(\mu_a + (1-g)\mu_s)} \nabla^2 \phi(r) = \text{Source Term} \quad (1)$$

where ϕ is the spatially varying light intensity, μ_a , μ_s , and g are the tissue absorption, scattering, and anisotropy coefficients at the emission wavelength, approximated with values from *in vivo* melanoma tissue,⁴⁴ and the source term for a point illumination source with intensity ϕ^0 and location r_1 is a delta function $\phi^0 \delta(r - r_1)$. For point sources in an unbounded medium, the Green's function is

$$G(\mathbf{r}) = \frac{3(\mu_a + (1-g)\mu_s)}{4\pi} \frac{\exp[-3\mu_a(\mu_a + \mu_s(1-g))|\mathbf{r}|]}{|\mathbf{r}|} \quad (2)$$

and the resulting spatiotemporal intensity for the illumination from all SWCNT point sources is a summation over the Green's function for each point source

$$\phi(\mathbf{r}, t) = \sum_k \phi_{0,k}(t) G(\mathbf{r} - \mathbf{r}_k(t)) \quad (3)$$

where $\phi_{0,k}(t)$ and $\mathbf{r}_k(t)$ are the time-dependent intensity and position of the k th SWCNT bundle. A point source was initially placed at every local maximum in the first frame of a nIR experimental movie and the closest sources combined until the minimum point separation was below a threshold distance of 5 μm (the length scale of interest). At each time frame T , we minimize the error between the frame pixels $I_{x,y}^T$ and the calculated intensity by adjusting the point intensity and locations

$$\min_{\phi_1^0(T), r_1(T), \phi_2^0(T), r_2(T), \dots} \sum_{x,y} [I_{x,y}^T - \phi(\mathbf{r} - (x, y), T)]^2 \quad (4)$$

An example of the resulting intensity field $\phi(\mathbf{r}, t)$ is shown in Figure 3C, as well as the point spread function $G(\mathbf{r})$ in the inset. Summation of the intensity field at each time point (Figure 3D), resulted in the same integrated information as discussed in Figure 2.

The local nitric oxide concentration at each sensor location can be calculated by considering the reversible interaction of NO with an unoccupied site on the SWCNT surface, forming the NO-SWNCT complex that results in a quenched emission state at that site, as we have shown previously in the case of single molecule detection⁴⁵ of NO. The adsorption and desorption of nitric oxide can be described by a first order reversible process, $\text{NO} + \text{SWCNT} \rightleftharpoons \text{NO-SWCNT}$ leading to the rate expression

$$\frac{d[\text{NO-SWCNT}]}{dt} = k_f[\text{NO}][\text{SWCNT}] - k_r[\text{NO-SWCNT}] \quad (5)$$

where k_f , k_r are the forward and backward rate constants, respectively, and calculated from previous *in vitro* single-SWCNT experiments²³ to be $k_f = 8.68 \times 10^{-4} (\mu\text{M s})^{-1}$ and $k_r = 3.18 \times 10^{-3} \text{ s}^{-1}$ (see Supporting Information Note 5). The SWCNT PL intensity is proportional to the fraction of unoccupied sites, $[\text{SWCNT}]$, or $I/I_0 = [\text{SWCNT}]/[\text{SWCNT}]_0$. The value of I_0 was set to correspond to the minimum initial NO concentration for the calculated concentrations to be positive, or $I_0 = I_{(t=0)}[1 + (k_f/k_r)C_0]$, where $C_0 = 5 \mu\text{m}$. The number of sensor sites are conserved with the conservation relation $[\text{SWCNT}]_0 = [\text{SWCNT}] + [\text{NO-SWCNT}]$. Making this substitution and rearranging, the concentration of NO can be calculated directly from the local intensity and its time-derivative

$$[\text{NO}] = \frac{1}{k_f} \frac{I_0}{I} \left[k_r \left(1 - \frac{I}{I_0} \right) - \frac{1}{I_0} \frac{dI}{dt} \right] \quad (6)$$

The finite imaging detector frame rate introduces noise into the calculation of the intensity derivative, potentially amplifying the fluctuations in the excitation source. Hence, each intensity trace is smoothed using a FFT low-pass filter prior to differentiation (Figure 3E). This method yielded similar results as compared to regularized differentiation⁴⁶ at a fraction of the computation cost. The resulting nitric concentrations are shown in Figure 3F for each of the SWCNT groupings in Figure 3C. Full analysis for each of the experimental conditions is included in Supporting Information Note 1. These NO concentrations fall within the same range as those reported in previous studies.³⁹ Complete analysis of nitric oxide concentration for all experimental conditions are included in the Supporting Information.

Previous work has shown that DNA-wrapped SWCNT enter the cell through macropinocytosis.³⁶ We found that the majority of A375 melanoma cells displayed fluorescent SWCNTs in multiple endosomes after a 3 h incubation. These allowed for the measurement of the heterogeneity of intracellular nitric oxide generation and decay (Figure 4). At each observed time point, the concentration difference between each pair of SWCNT sensors was calculated and normalized by their spatial separation. All of the observed differences over the course of an experiment were used to build a probability density of concentration differences (Figure 4A). Before stimulation with JS-K, difference values of approximately $0.1 \mu\text{M}/\mu\text{m}$ were observed, corresponding to baseline intracellular NO heterogeneity. When $28 \mu\text{M}$ of JS-K was added, NO differences increased to $1 \mu\text{M}/\mu\text{m}$. This change is potentially due to a combination of variations in JS-K diffusion into the cell and intracellular glutathione (see Figure 3F). Over time, the observed differences returned to their values before JS-K addition.

The diffusion of nitric oxide has been very well studied. For a diatomic gas with a diffusion coefficient of $10^{-7} \text{ cm}^2/\text{s}$, equilibrium can be achieved on the order of 10 ms. However, our setup detects intracellular concentration differences persisting over seconds. We demonstrate below that such spatial and temporal fluctuations can only occur from the asynchronous modulation of two or more spatially distinct NO sinks within the cell. These results can be understood with a

simple numerical model for JS-K diffusion and reaction to produce nitric oxide within the cell.

Numerical Model for the Response of Intracellular SWCNT to an External JS-K Stimulus. To understand the implications of the nitric oxide gradients reported by our sensors under a variety of conditions, we constructed a simple numerical 2D model for the diffusion of JS-K into the cell and the reaction with GSH to form NO according to the scheme presented in Figure 1D. We also consider various models for spatially heterogeneous production and consumption of intracellular NO that have not yet been considered due to the lack of NO sensors with sufficient spatial resolution.

We construct a diffusion and reaction model to simulate intracellular nitric oxide (NO) concentrations from JS-K treatment (see Supporting Information Table 1 for model parameters and Supporting Information Note 2 for full details of the model). The geometry of the system simulates the cytosol with a $10 \mu\text{m}$ diameter circle and a nucleus at the center with a $2 \mu\text{m}$ diameter impermeable boundary (Figure 4). The outer boundary of the cytosol was permeable to JS-K and NO but impermeable to GSH. The concentration of JS-K was set outside the cell to the various levels used in the experiments ($16\text{--}28 \mu\text{M}$). The reaction of JS-K with GSH to form NO was included with literature rate data.⁴⁰ Intracellular NO production and first-order consumption was modeled both homogeneously and heterogeneously with sources and sinks as two-dimensional sinusoidal functions (i.e., proportional to $[\sin(x/X)\sin(y/Y)]^a$, where we control the sharpness and position of the function with a , x , and y). The magnitudes of these functions were adjusted to obtain the experimental concentrations of NO and the resulting intracellular spatial differences were compared. COMSOL was used to solve for the resulting NO concentrations and each simulation was run until equilibrium was reached, typically 10 s.

We performed the simulation for combinations of four potential sources placed either proximal or distal to the nucleus (Figure 4B). Random pairs of points were used to calculate the gradient in the perinuclear region, defined as between 1 and $3 \mu\text{m}$ to the center of the simulated cell. A kernel density estimation of the gradient probability density distribution was constructed to compare with the experimental readings (Figure 4C,D). At least one sink that caused a polarization of the intracellular NO concentrations was required to result in gradients similar to those reported by our intracellular sensors. Furthermore, while proximal sources created higher gradient readings, probability density function shapes from sources further away from the nucleus more closely resembled the data. We hypothesize that the sensors are detecting multiple GSH sources at different intracellular locations during the experiment. Future work will focus on the identification and characterization of cellular sources of NO. As SWCNT sensors can be modified to detect a variety of species, this intracellular detection schema can be used to understand the distribution and modulation of other biological molecules.

The role of NO in human physiology and pathology is paradoxical not only in its contributions to vasodilation, neurotransmission, and intercellular signaling but also its implications in DNA damage, lipid oxidation, and cancer progression. One prevailing hypothesis explaining this paradox attributes the NO associated pathway and outcome to local concentrations on the tissue or cellular scale. It is important to note that current detection systems potentially yielding such spatial information either do not have the required resolution

or fail to measure NO directly. Therefore, the field currently lacks the appropriate tools to test the above hypothesis.

The method we developed in this work along with our findings call into question the notion of an average cellular concentration of NO. We show clear evidence for persistent gradients within the cell. These gradients are observed with both exogenous (JS-K) and endogenous (VEGF → eNOS) NO sources. We believe that these gradients are a result of sources and sinks nonuniformly distributed within the cell. With gradients of the magnitude that we observe, regions of the cell will experience NO concentrations at orders of magnitude higher than others. This phenomenon and its regulation can be important in NO signaling and is not reflected in current bulk detection systems. Even more importantly, we show that this gradient fluctuates in tens of seconds and that this can only arise from temporal modulations in the source and sink pathways for NO. As biological signaling is often modulated via duration and frequency, deciphering intracellular NO dynamics can prove to be instrumental in studying the mechanism of NO action for its various biological functions.

We use d(AT)₁₅-DNA in this work to demonstrate the intracellular detection of NO. In comparison with other techniques, the preparation of SWCNT probes is relatively simple and does not require organic synthesis. These sensors are stable for prolonged periods of time and do not photobleach with repeated excitation at high frequency. Furthermore, nIR imaging allows for minimal signal attenuation in biological environments that also lends itself to tissue analysis in addition to *in vitro* culture. For the first time, we were able to achieve intracellular spatial and temporal NO resolution. In addition to concentration, we show that location and frequency of NO signals can now be detected and may play a major role in intra- and extracellular communication.

Overall, this technology allows for the study of NO that will further our understanding of its function in cellular signaling and equilibrium. It can also be readily expanded for the detection of other species and multiplexed for multiplex applications. In this case, investigation of NO dynamics can extend to applications such as the early detection of endothelial dysfunction and the study of tumor progression and response to treatment. As a unique tool to query cellular states, these sensors provide new and valuable information in both the basic understanding and potential toward novel clinical diagnostics.

■ ASSOCIATED CONTENT

Supporting Information

Supplemental figures with comparison to results using the DAF-FM dye, calibration data for the GSH concentration reported in this work, full spatiotemporal analysis for each experimental condition reported in this work. Supplementary notes describing the spatiotemporal analysis data, the numerical reaction-diffusion model, additional verification experiments, GSH calibration methods, supporting kinetic data and rate constants, description of DAF-FM protocols for comparison, and a full list of experimental methods and chemical preparation steps. This material is available free of charge via the Internet at <http://pubs.acs.org>.

■ AUTHOR INFORMATION

Corresponding Author

*E-mail: strano@mit.edu. Phone: 617-324-4323. Fax: 617-324-4323.

Present Address

[#]New Addresses. Department of Chemical Engineering, California Institute of Technology, Pasadena, CA, 91125, USA.

Author Contributions

[#]Z.W.U., F.S., and X.G. contributed equally.

M.S.S., F.S., X.G., and Z.W.U. wrote the paper with input from D. M. Experiments were carried out by F.S., S.S., and X.G. Experimental data analysis provided by Z.U. and X.G. Z.U. developed optical modeling and sensor tracking, and X.G. performed numerical COMSOL simulations. A.B. assisted with experimental setup and measured the NO/SWCNT adsorption/desorption kinetics. N.I. and L.G. assisted with cell culturing and uptake. G.W. provided insight into intracellular NO mechanisms and developing necessary experimental controls. All authors have given approval to the final version of the manuscript.

Notes

The authors declare no competing financial interest.

■ ACKNOWLEDGMENTS

This work was supported by a grant from the National Science Foundation to M.S.S. Z.W.U. acknowledges support from the DOE CSGF program (DOE Grant DE-FG02-97ER25308). X.G. acknowledges support from the National Institute of General Medical Sciences (T32 GM 65841 and T32 ST32CA148073). D.M. acknowledges NIH Grants HL70567 and CA150190. F.S. acknowledges support from the DPU-ILTEM. A.A.B. acknowledges support by Department of Defense (DoD) through the National Defense Science & Engineering Graduate Fellowship (NDSEG) program.

■ ACKNOWLEDGMENTS

We acknowledge Julie Lau for editing the manuscript.

■ ABBREVIATIONS

SWCNTs, single-walled carbon nanotubes; PL, photoluminescence; HUVEC, human umbilical endothelial cells; GSH, glutathione; JS-K, O₂-(2,4-dinitrophenyl)-1-[4-(ethoxycarbonyl)piperazin-1-yl]diazen-1-ium-1,2-diolate; NO, nitric oxide; eNOS, endothelial nitric oxide synthase

■ REFERENCES

- (1) Ignarro, L. J. *Nitric Oxide: Biology and Pathobiology*, 2 ed.; Academic Press: Burlington, MA, 2009; p 845.
- (2) MacMicking, J.; Xie, Q. W.; Nathan, C. *Annu. Rev. Immunol.* **1997**, *15*, 323–50.
- (3) Coussens, L. M.; Werb, Z. *Nature* **2002**, *420* (6917), 860–867.
- (4) Dedon, P. C.; Tannenbaum, S. R. *Arch. Biochem. Biophys.* **2004**, *423* (1), 12–22.
- (5) Muniyappa, R.; Quon, M. *Curr. Opin. Clin. Nutr. Metab. Care* **2007**, *10*, 523–530.
- (6) Fukumura, D.; Kashiwagi, S.; Jain, R. K. *Nat. Rev. Cancer* **2006**, *6* (7), 521–34.
- (7) Barta, C.; Kálai, T.; Vass, I.; Hideg, K.; Hideg, É. *Acta Biol. (Szeged)* **2002**, *46*, 149–150.
- (8) Bell, E. L.; Klimova, T. a.; Eisenbart, J.; Schumacker, P. T.; Chandel, N. S. *Mol. Cell. Biol.* **2007**, *27*, 5737–45.
- (9) Lim, M. H.; Xu, D.; Lippard, S. J. *Nat. Chem. Biol.* **2006**, *2*, 375–80.
- (10) Michelakis, E. D. *Circ. Res.* **2002**, *90*, 1307–1315.
- (11) Miller, E. W.; Albers, A. E.; Pralle, A.; Isacoff, E. Y.; Chang, C. J. *J. Am. Chem. Soc.* **2005**, *127*, 16652–9.
- (12) Schrand, A. M.; Braydich-Stolle, L. K.; Schlager, J. J.; Dai, L.; Hussain, S. M. *Nanotechnology* **2008**, *19*, 235104.

- (13) Wei, Z.; Al-mehdi, A. B.; Fisher, A. B. Signaling pathway for nitric oxide generation with simulated ischemia in flow-adapted endothelial cells. *Am. J. Physiol.: Heart Circ. Physiol.* **2001**, *281* (5), H2226–H2232.
- (14) Liu, J.; Roussel, C.; Lagger, G.; Tacchini, P.; Girault, H. H. *Anal. Chem.* **2005**, *77*, 7687–94.
- (15) Lvovich, V.; Scheeline, A. *Anal. Chem.* **1997**, *69*, 454–462.
- (16) Tang, M.; Chen, S.; Yuan, R.; Chai, Y.; Gao, F.; Xie, Y. *Anal. Sci.* **2008**, *24*, 487–91.
- (17) Varfolomeev, S. *Biosens. Bioelectron.* **1996**, *11*, 863–871.
- (18) Wilson, R. C. K.; Phuong, D. T.; Chainani, E.; Scheeline, A. J. *Electroanal. Chem.* **2011**, *2*–6.
- (19) Zhang, X.; Kim, W.-S.; Hatcher, N.; Potgieter, K.; Moroz, L. L.; Gillette, R.; Sweedler, J. V. *J. Biol. Chem.* **2002**, *277* (50), 48472–48478.
- (20) Alivisatos, A. P.; Gu, W. W.; Larabell, C. Quantum dots as cellular probes. In *Annual Review of Biomedical Engineering*; Annual Reviews: Palo Alto, 2005; Vol. 7, pp 55–76.
- (21) Wang, Y.; Li, Z.; Wang, J.; Li, J.; Lin, Y. *Trends Biotechnol.* **2011**, *29* (S), 205–212.
- (22) Mayer, K. M.; Hafner, J. H. *Chem. Rev.* **2011**, *111* (6), 3828–3857.
- (23) Zhang, J.; Boghossian, A. A.; Barone, P. W.; Rwei, A.; Kim, J.-H.; Lin, D.; Heller, D. A.; Hilmer, A. J.; Nair, N.; Reuel, N. F.; Strano, M. S. *J. Am. Chem. Soc.* **2010**, *133* (3), 567–581.
- (24) Barone, P. W.; Baik, S.; Heller, D. A.; Strano, M. S. Modulating single walled carbon nanotube fluorescence in response to specific molecular adsorption. *AIP Conf. Proc.* **2005**, 193.
- (25) Barone, P. W.; Baik, S.; Heller, D. A.; Strano, M. S. *Nat. Mater.* **2004**, *4* (1), 86–92.
- (26) Barone, P. W.; Parker, R. S.; Strano, M. S. *Anal. Chem.* **2005**, *77* (23), 7556–7562.
- (27) Barone, P. W.; Strano, M. S. *Angew. Chem.* **2006**, *118* (48), 8318–8321.
- (28) Heller, D. A.; Jeng, E. S.; Yeung, T.-K.; Martinez, B. M.; Moll, A. E.; Gastala, J. B.; Strano, M. S. *Science* **2006**, *311* (5760), 508–511.
- (29) Jeng, E. S.; Barone, P. W.; Nelson, J. D.; Strano, M. S. *Small* **2007**, *3* (9), 1602–1609.
- (30) Jeng, E. S.; Moll, A. E.; Roy, A. C.; Gastala, J. B.; Strano, M. S. *Nano Lett.* **2006**, *6* (3), 371–375.
- (31) Jin, H.; Jeng, E. S.; Heller, D. A.; Jena, P. V.; Kirmse, R.; Langowski, J.; Strano, M. S. *Macromolecules* **2007**, *40* (18), 6731–6739.
- (32) Jin, H.; Heller, D. A.; Kalbacova, M.; Kim, J.-H.; Zhang, J.; Boghossian, A. A.; Maheshri, N.; Strano, M. S. *Nat. Nanotechnol.* **2010**, *5* (4), 302–309.
- (33) Kim, J.-H.; Patra, C. R.; Arkalgud, J. R.; Boghossian, A. A.; Zhang, J.; Han, J.-H.; Reuel, N. F.; Ahn, J.-H.; Mukhopadhyay, D.; Strano, M. S. *ACS Nano* **2011**, *5* (10), 7848–7857.
- (34) Kim, J.-H.; Heller, D. A.; Jin, H.; Barone, P. W.; Song, C.; Zhang, J.; Trudel, L. J.; Wogan, G. N.; Tannenbaum, S. R.; Strano, M. S. *Nat. Chem.* **2009**, *1* (6), 473–481.
- (35) Iverson, N. M.; Barone, P. W.; Shandell, M.; Trudel, L. J.; Sen, S.; Sen, F.; Ivanov, V.; Atolia, E.; Farias, E.; McNicholas, T. P.; Reuel, N.; Parry, N. M. A.; Wogan, G. N.; Strano, M. S. *Nat. Nanotechnol.* **2013**, *8* (11), 873–880.
- (36) Bhattacharya, S.; Roxbury, D.; Gong, X.; Mukhopadhyay, D.; Jagota, A. *Nano Lett.* **2012**, *12*, 1826–30.
- (37) Iwakiri, Y.; Satoh, A.; Chatterjee, S.; Toomre, D. K.; Chalouni, C. M.; Fulton, D.; Groszmann, R. J.; Shah, V. H.; Sessa, W. C. *Proc. Natl. Acad. Sci. U.S.A.* **2006**, *103* (S2), 19777–82.
- (38) Tvrdy, K.; Jain, R. M.; Han, R.; Hilmer, A. J.; McNicholas, T. P.; Strano, M. S. *ACS Nano* **2013**, *7* (2), 1779–1789.
- (39) Chin, M. P.; Deen, W. M. *Nitric Oxide* **2010**, *23* (4), 319–326.
- (40) Shami, P. J.; Saavedra, J. E.; Wang, L. Y.; Bonifant, C. L.; Diwan, B. A.; Singh, S. V.; Gu, Y.; Fox, S. D.; Buzard, G. S.; Citro, M. L.; Waterhouse, D. J.; Davies, K. M.; Ji, X.; Keefer, L. K. *Mol. Cancer Ther.* **2003**, *2* (4), 409–417.
- (41) Kasherman, Y.; Sturup, S.; Gibson, D. *J. Med. Chem.* **2009**, *52* (14), 4319–4328.
- (42) Drew, R.; Miners, J. O. *Biochem. Pharmacol.* **1984**, *33* (19), 2989–2994.
- (43) Kroll, J.; Waltenberger, J. *Biochem. Biophys. Res. Commun.* **1998**, *252* (3), 743–746.
- (44) Garcia-Uribe, A.; Smith, E. B.; Zou, J.; Duvic, M.; Prieto, V.; Wang, L. V. *J. Biomed. Opt.* **2011**, *16* (2), 020501–020501–3.
- (45) Boghossian, A. A.; Zhang, J.; Floch-Yin, F. T. L.; Ulissi, Z. W.; Bojo, P.; Han, J.-H.; Kim, J.-H.; Arkalgud, J. R.; Reuel, N. F.; Braatz, R. D.; Strano, M. S. *J. Chem. Phys.* **2011**, *135* (8), 084124.
- (46) Stickel, J. J. *Comput. Chem. Eng.* **2010**, *34* (4), 467–475.